Millimeter-Wave Information-Centric Wireless-Sensor-Network Ecosystem: Evaluation under Non-Terrestrial and Long-Distance Environments in Actual City

Shintaro Mori
Department of Electronics Engineering and Computer Science
Fukuoka University
8-19-1 Nanakuma, Jonan-ku, Fukuoka 814-0180, Japan
E-mail: smori@fukuoka-u.ac.jp

Abstract — **This paper presents an evaluation of the previously presented information-centric wireless-sensor-network-based framework for smart-city applications, called mmICWSN. The framework uses millimeter-wave communications for future broadband wireless networks. To demonstrate the feasibility, the network performance, including application and network-layer throughput, was evaluated, and the video-streaming application was demonstrated in a non-terrestrial environment and in an actual city. In addition, the computer simulations are also performed. The experiments were conducted in the KOIL mobility field (Chiba, Japan) and Nogata City (Fukuoka, Japan). The demonstrations include the proof of concept for constructing a wireless network via multiple aerial nodes and establishing long-range wireless links in an actual city, connecting two 1-km-distant locations. The results indicate that our ecosystem can be verified to communicate with a point-to-point environment.**

Keywords-information-centric wireless sensor network; millimeter-wave communications; smart-city ecosystem.

I. INTRODUCTION

Internet of Things (IoT) and Wireless Sensor Network (WSN) technologies are essential and foundational for supporting smart-city applications to collect and distribute sensing data [2]. Traditional host-centric networking framework has limitations in managing sensing data due to addressing, inefficient mobility support, and unsophisticated in-network caching. Building IoT on top of Information-Centric Networking (ICN) [3][4] is believed to be a promising solution to tackle the above issues. ICN is an ideal candidate for future network architecture that shifts the focus from host locations to data. In short, ICN names data rather than addresses; hence, end-users can discover and obtain data on the basis of name, resulting in network abstraction. The data are copied and stored in cache memory for subsequent retrievals and can be self-certified and encrypted to improve security.

Underpinning future smart-city applications, wide-band and low-latency wireless communications will be necessity, thereby motivating to explore higher-frequency bands. In other words, it is necessary to consider using not only both Microwave bands (microWave) and Sub-gigahertz bands (sub-gigahertzWave), but also Millimeter wave bands (mmWave) [5]. Currently, mmWave-band radio is primarily used for radar and academic astronomy, while wireless communication is not so popular.

In the previous studies, a mmWave Information-Centric Wireless Sensor Network (mmICWSN) framework has been investigating and the framework integrates the three technologies, such as mmWave, ICN, and WSNs[6][7][8]. Among them, the mmICWSN test field was implemented and a preliminary evaluation was performed [6]. For practical operational demonstrations, long-term operational testing was conducted at the same field [7]. Through the experiments, serious weather effects in mmWaves were not observed, and the beam angle had a greater impact on network performance. In addition, a ground-to-air mmWave experiment using a single drone was conducted, assuming a Non-Terrestrial network (NTN) environment [8].

This paper addresses the following two matters that are insufficiently investigated in these studies, i.e., multi-hop air-to-air mmWave communications and experimental verification of long-distance mmWave communications. The baseline paper [1] presented some network-performance results; in this paper, additional evaluation results for an aerial multi-hop scenario and computer simulations are provided.

The remainder of this paper is organized as follows. Section II discusses related work. Section III provides a brief overview of the mmICWSN. Sections IV and V present the experimental evaluation results of the NTN environment and the long-distance demonstration, respectively. Sections VI presents the computer simulation result regarding IEEE 802.11 ad/ay-based communications to complement the experimental results. Finally, Section VII concludes this paper with a summary and mention of future work.

II. RELATED WORK

In the ecosystems of smart cities, IoT technology is an essential component due to its ability to utilize sustainable information and communication technologies [9]. As a wireless communication system underpinning smart-city application services, a comprehensive review and survey of the future evolution of next-generation technologies, including their principles, potential applications, current state-of-the-art research, and the related technical challenges, was surveyed [10][11][12]. The wireless backhaul has become a key enabler for future mobile communications systems, offering a cost-effective and scalable alternative to traditional fiber backhaul. Thanks to the availability of high bandwidths, data can be transmitted over fiber; however, the higher radio-

frequency bands suffer from propagation loss, distortion, and blockage. Ferreira et al. [13] presented an extensive measurement campaign and cross-layer analysis for outdoor mmWave environments. Doone et al. [14] used a commercial ray tracing engine to investigate two hypothetical use cases within future factories, such as inventory monitoring using an UAV and movement of stock using a forklift vehicle at microWaves and mmWaves.

Regarding the network performance of mmWaves, Zhang et al. [15] and Khorov et al. [16] surveyed the open challenges for transport- and network-layer protocols on the basis of a comprehensive simulation study. In particular, transport- and network-layer protocols are unsuitable for mmWaves because of their specific features compared with those of commonly used bands, due to high signal attenuation and blockage. Kumar et al. [17] experimentally found throughput degradations (collapses) in the 60-GHz band (one of the key frequency bands for mmWaves). Poorzare et al. [18] analyzed network performances related to this phenomenon under an urban deployment scenario.

Regarding ICN technology for smart-city applications, current implementation proposals for ICN-based IoT, as well as the caching and replacement policies presented, were surveyed [19]. Safitri et al. [20] proposed a mobile IoT optimization method for next-generation networks by evaluating a series of name-based techniques implemented in ICN. Gur et al. [21] found that consolidating ICN with MEC technology offers new opportunities to realize that vision and serve advanced use cases.

III. MMWAVE INFORMATION-CENTRIC WIRELESS SENSOR NETWORK FRAMEWORK

Figure 1 shows the network structure of the mmICWSN framework. In the framework, there are three types of network nodes: Private Base Station (PBS), Relay Node (RN), and Sensor Node (SN). PBS is a coordinator that manages a regional (local) network deployed in the field, and it acts as a gateway to external networks. RNs use mmWaves for backhaul and can be further classified into Ground RNs (GRNs) and Aerial RNs (ARNs) based on node location, such as NTNs. GRN provides high-performance relay functions under commercial power supply, while ARN mediates sensing data from ground-based SNs via Unmanned Aerial Vehicles (UAVs) with battery power.

On the other hand, RNs can be alternatively classified into mmRN and μRN, which utilize radio wavelengths at mmWaves and microWaves, respectively. The mmRN is a repeater node that enables high-speed wireless mesh networks to replace optical fiber networks in the field. If we construct a network using only mmRN, the construction costs will be expensive, and backward compatibility cannot be guaranteed. To mitigate this situation, μRN can promotes a low-cost deployment, enabling the usage of the 6-GHz band as well as the 5-GHz band. SNs are deployed in the field, and the sensing data are packaged and posted to the network. Sensing data includes not only text-based data, such as temperature, humidity, and illuminance, but also large-sized data, such as images, videos, and 3D sensing data. In addition, the data includes not only data that can tolerate delays, but also real-time and delay-sensitive data.

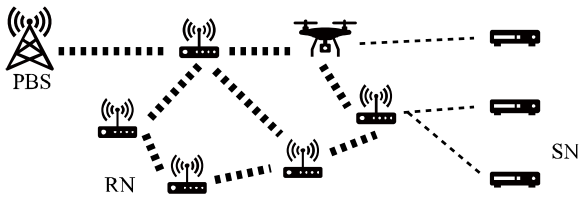

Figure 1. Network model of the mmICWSN framework

Regarding the selection of wireless communication systems for smart cities, particularly for outdoor environments such as smart agriculture, there are several options. Namely, there are cellular and satellite networks, Low-Power Wide-Area Networks (LPWANs), Personal Area Networks (PANs), Wireless Local Area Networks (WLANs), and, exceptionally, optical wired networks [22][23][24]. These network systems have both strengths and weaknesses; therefore, it is necessary to determine where they are suitable for deployment in terms of communication coverage, network communication (wireless) capacity, and the economic and technical costs of implementation, construction, and deployment.

Cellular and satellite telecommunications are the de facto systems, but their operation costs are high. LPWANs, such as LoRa and SigFox, have been widely adopted to provide wide-area coverage and low energy consumption. However, LPWANs are generally assigned 100-Hz bandwidth in the sub-gigahertz band; thus, the system can only transfer small amounts of data. PANs are used as traditional WSNs, but the deployment is limited to environments inside small-area networks. The wired network is the primary choice in areas where optical fiber lines have already been deployed; however, deploying new optical lines is unrealistic in rural areas due to economic reasons.

In contrast, the mmICWSN framework adopted the network structure of WLANs based on the IEEE 802.11 standard, also known as Wi-Fi (certified by its alliance). WLANs are widely recognized as another global communication system in comparison with cellular networks. In addition, the network system has several advantages, including low-cost wireless modules readily available, the ability to be constructed on IP networks, and the availability of unlicensed radio-frequency bands without regulations.

IV. EXPERIMENTAL RESULTS OF THE NTN ENVIRONMENT

In this section, we present a demonstration and an experiment on backhaul network construction using ARNs to answer the fundamental question: whether a high-speed wireless link can be established among aerial networks. The experiment was conducted in a simulated drone environment, using smart poles rather than actual drones, to demonstrate the feasibility of deploying multiple ARNs. In addition to evaluating fundamental network performance, we conducted video streaming trials to demonstrate that the mmICWSN framework can support delay-sensitive applications.

A. Experimental environment and setup

The experiment was conducted in the KOIL mobility field (Chiba, Japan), and its field view is shown in Figures 2 and 3. As shown in Figure 4, the field consists of three areas: a paved road for autonomous vehicle testing, a gravel (ballast) area for heavy vehicle testing, and a grass (weed) area for agricultural machinery testing. In the experiment, to deploy backhaul networks among mmRNs, we used Terragraph [25], which Meta (Facebook) offered as an mmWave mesh network to deploy an IEEE 802.11 ay-compliant network. Distribution Nodes (DNs) and Client Nodes (CNs) are used. With multiple DNs are interconnected to form a backhaul network that enables end-users to access the network via CNs. Note that Terragraph can communicate with DNs and CNs via multi-hop transmissions with a maximum of 15 hops, and the router node supports the Open/R routing protocol. In addition, Terragraph is compatible with the IEEE 802.11 ad/ay specification, but the device we used (BeMap MLTG-360 as a DN and MLTG-CN [26]) only supported single-carrier modulation at the physical layer.

Regarding the wireless communication devices, the maximum Effective Isotropic Radiated Powers (EIRP) are 43 dBm (DN) and 38 dBm (CN) at the transmitter, and the antenna gains are 28 dBi (DN) and 22 dBi (CN), respectively. In particular, their antenna consists of a phased array with 64 elements, and the steering angular ranges are [−45°, 45°] in the azimuth plane (φ) and [−25°, 25°] in the elevation plane (θ). Under Japan's Radio Act, Terragraph is assigned the unlicensed 60-GHz band (57–66 GHz) with four channels: 58.32, 60.48, 62.64, and 64.80 GHz (central) frequency bands, each with a 2.16-GHz bandwidth. For the ICN platform, we used Cefore [27], an open-source CCNx-based platform available on Linux (Ubuntu). Cefore consists of two daemon processes: cefnetd and csmgrd. Namely, cefnetd exchanges the data and forwards interest packets, and csmgrd provides an in-network caching scheme.

To experiment in the NTN environment, we utilized smart poles [28]. This smart-pole-based airspace testbed validates the feasibility of drone networks and services in real-world settings, as illustrated in Figure 3. The smart-pole platform was utilized for several practical reasons, such as field restrictions and the high cost of drones. The smart pole has several propellers that can simulate drone movement, as shown in Figure 3(a). The smart pole requires two or more persons to lift it up, but it can stand on its own once the propellers are rotated. Namely, the propeller rotation can be automatically controlled to maintain stability by adjusting the angle of the pole, as shown in Figure 3(b).

The experimental devices were arranged in two layouts: all devices in a straight line (Figure 4(a)) and the smart poles at 90-degree angles to each other, forming a zigzag pattern (Figure 4(b)). Smart poles were placed on the gravel areas, and an SN was placed on the paved road. The distance between each wireless node was set to 11.7–29.4 m, which is summarized in Figure 4. For the three wireless sections, we have assigned a radio channel from four channels specified in IEEE 802.11 ay without any overlap, and we have suspended any other mmWave network in the field to prevent radio-wave interference. The reasons for assuming these layouts are as follows. When ARN mediates SN in cooperation with GRNs that are placed in a grid (lattice) pattern around the field, the scenario involves UAVs being aviated along the vertical (or horizontal) lines. The scenario where all devices are placed in a straight line is reasonable for this situation. On the other hand, for the zigzag pattern, when the GRNs that are usually connected to the ARN cannot transfer data, another neighbor GRN will be switched.

Figure 2. Field view of experimental site in the KOIL mobilty field

(a) (b)

Figure 3. Smart pole in which a city airspace testbed system

Figure 5 shows the experimental network. As a PBS, Terragraph DN was placed on the fixed pole. We used a PC with Ubuntu installed on a Microsoft Surface as a user terminal, and the PC was connected to the PBS. The network links, including air-to-air and air-to-ground, were three-hop mmWaves. The pair of communication devices was utilized with two Terragraph CNs on the pole head, as shown in Figure 3(a). Since the weight limit for pole loadable, the mobile battery for power supply, and the control computer are located on the ground. The antenna was set to 4.2 m height, and its surface was oriented toward the opposite device. SN was used to implement a node with a web camera and CN.

B. Experimental results: Network performance

Figure 6 shows the experimental results, which include both (a) and (b), (c) and (d), and (e) and (f), respectively, for

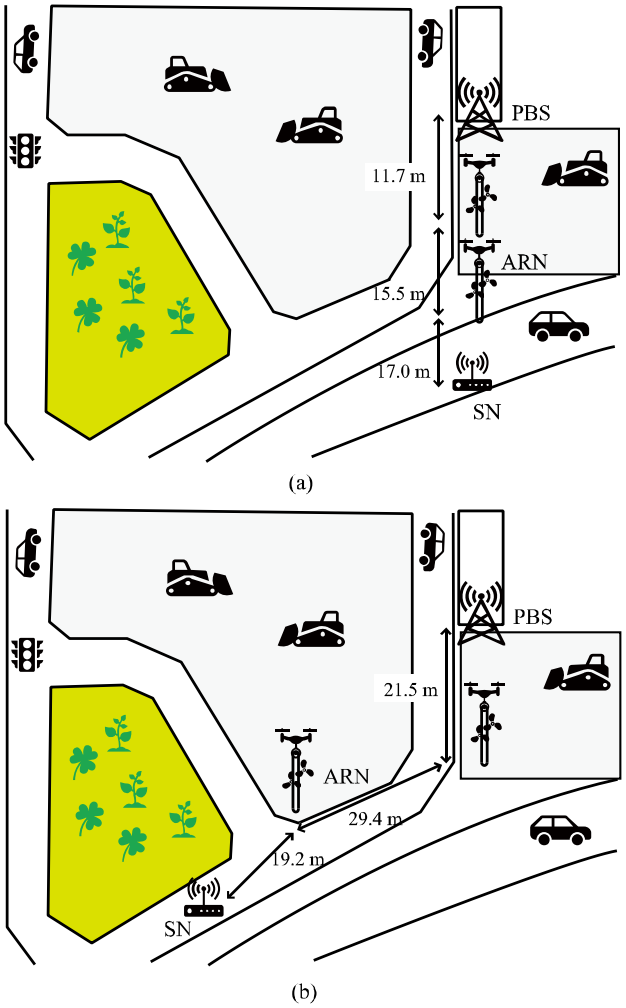

Figure 4. Field layout and node placement

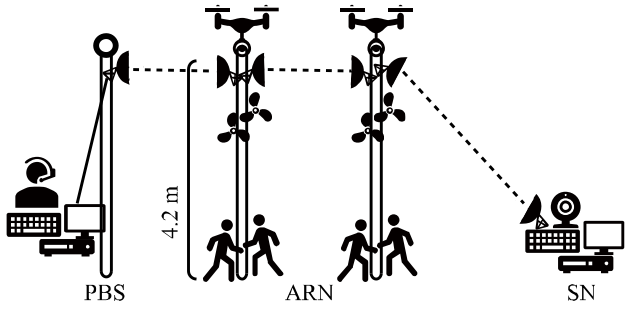

Figure 5. Experimental netowrk for mmWaves among ARNs

Transmission Control Protocol (TCP) with the CUBIC algorithm, User Datagram Protocol (UDP), and ICN performance. In Figures 7(a) to (d), iPerf3 [29], a well-known network-performance measurement tool, was used to measure TCP/UDP performance at 1 s interval for 90 s. Figures 6(e) and (f) show the results of retrieving the different data using Cefore.

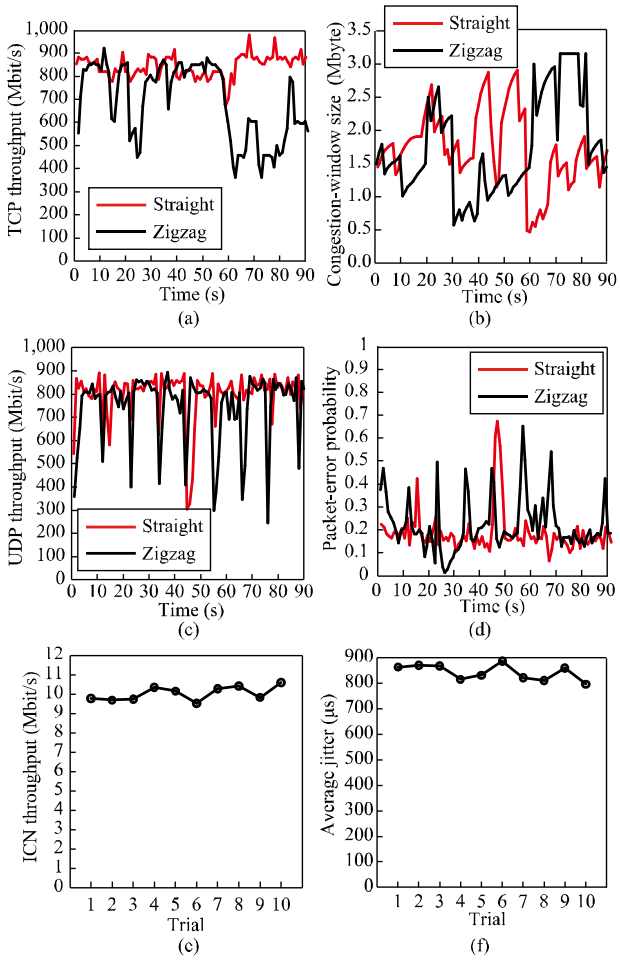

Figure 6. Experimental results regarding network performance in the NTN environment

As shown in Figure 6(a), the average TCP throughput was 841 and 693 Mbit/s for straight and zigzag placements, respectively. Compared to the TCP throughput of straight placement, that of zigzag was 17.7% lower, but it remained above several hundred megabits per second. For TCP congestion control, as shown in Figure 6(b), the average congestion-window size were 1.72 and 1.75 Mbytes; hence, there was no significant difference. As shown in Figure 6(c), the average UDP throughput was 805 and 752 Mbit/s for the two placements, respectively. Figure 6(d) shows the packet-error probability for UDP transfer; the averages were 0.193 and 0.225 for the two placements, respectively, in which there was no significant difference. As shown in Figure 6(e), the average ICN throughput was 10.0 Mbit/s for the straight placement. As shown in Figure 6(f), the average jitter was 843 μs for the straight placement. ICN throughput and jitter did not significantly differ between the two scenarios. In addition, the ICN throughput was significantly smaller than that of TCP or UDP because Cefore has a bottleneck. We also experimentally verified that we could obtain sufficient network performance for mmICWSN via multiple ARNs.

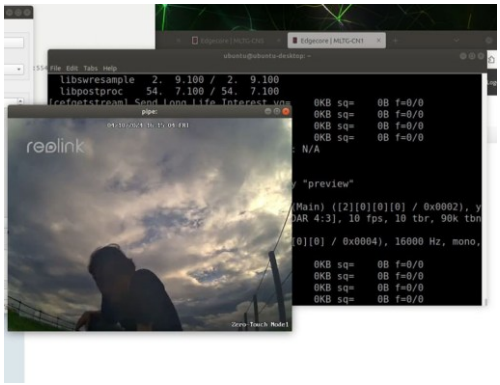

Figure 7. Experimental results regarding video-streaming demonstration in the NTN environment

Figure 8. Location map of transmitter- and receiver-side nodes

C. Experimental results: Video-streaming demonstration

In the experiments of this section, the camera video equipped with the SN device, shown in Figure 5, was retrieved as streaming data at the user terminal. Unlike the previous section's experiment, the cefgetstream and sefputstream commands in Cefore were used to transmit and retrieve real-time video streams. Note that, to integrate Cefore into the device, we can register and obtain the data from the application software using the following commands: cefputfile and cefgetfile for sending and receiving static data, respectively. Figure 7 shows the results of the video streaming experiment. The results show that the video can be delivered smoothly over the three-hop mmWave links in air-to-air environment. In addition, with the availability of video streaming applications, the mmICWSN framework can be effective for several applications requiring low-latency data flow.

V. Experimental Results of Long-Distance Communications in Actual City

As another proof-of-concept experiment in this paper, the feasibility of long-distance communication in an actual city deployment was evaluated. To develop ecosystems in actual cities, additional evaluations are necessary. To the best of our knowledge, there have been few experiments on mmWave long-distance data transmission; therefore, this paper's contribution is valuable.

A. Experimental environment and setup

The node devices were deployed at a community center and school in Nogata City (Fukuoka, Japan), as shown in Figure 8. The community center and school are three-story buildings, and the node devices were placed on their rooftops. In accordance with the three-dimensional map provided by the National Geographical Institute [30], their altitudes are respectively 7.5 and 16 m, and the straight-line distance between them is 1 km. Across the wireless link, there is a river, a road, a bridge, and a car park, as shown in Figure 9, which might affect radio propagation. The river is the Onga River and the riverside area is well maintained and covered with

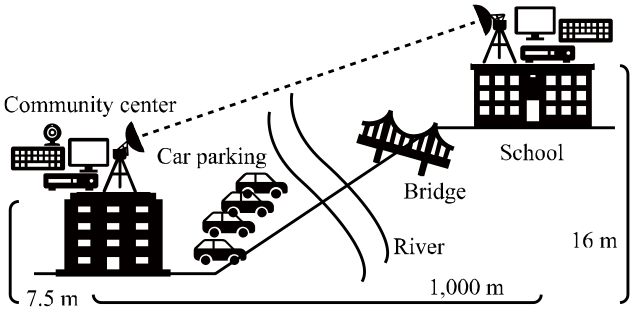

Figure 9. Outline of experimental environment regarding long-distance testing

grass and aquatic plants. During the experiment, the river surface was flat and calm, with no significant waves, i.e., factors affecting mmWaves propagation were not observed. The Kanroku Bridge spans the river and connects to the main national road. Nogata City is an inter- and suburban city between large cities (e.g., Fukuoka City and Kitakyushu City), but traffic is not dense. The riverside area in front of the community center is used as a parking lot, with several dozen cars parked there.

Figure 10 shows the field view of the experimental site. Figures 10(a) and (b) and Figures 10(c) and (d) show the field views of the rooftops of the community center and school, respectively. As shown in Figures 10(a) to (d), the mmICWSN node devices were connected to the Terragraph devices. In the experiment, two MLTG-CNLR devices communicated over distances up to 1 km, as specified in the catalog. In the MLTG-CNLR device, the EIRP is 56 dBm, and the antenna gain is 40 dBi. In addition, the MLTG-CNLR's antenna is a dish (parabola) type, and its scan range and beam width are 3° and 1°, respectively (that is, narrow compared with the former two devices). Throughout the experiment, the Modulation and Coding Scheme (MCS) index was automatically set as 9. Table I shows the parameter settings regarding adaptive rate control in the IEEE 802.11 ay. Note that IEEE 802.11-compliant Wi-Fi systems achieve effective (high-throughput) data transmission using the control modulation scheme, the error-correcting code rate, and a

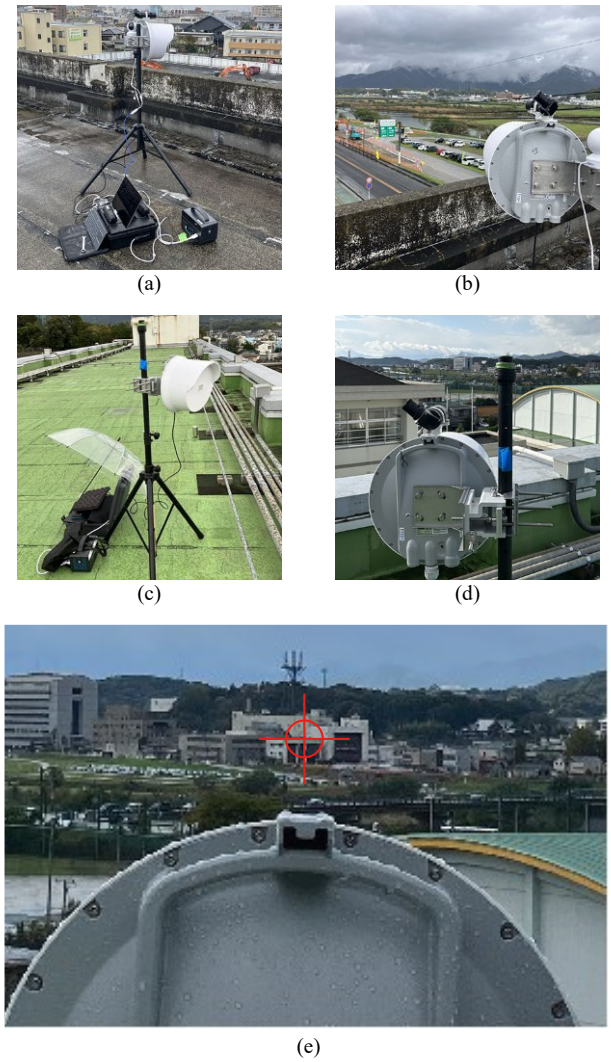

Figure 10. Field view of transmitter- and receiver-side nodes on rooftop of community center and school buildings

repetition code based on the wireless channel condition, and their combination is predefined as the MCS settings.

Figure 10(e) shows a photo taken behind the dish antenna on the school rooftop toward the community center. The community center is located at the red marking, where the opposite node was placed. As shown in Figure 10(e), the line of sight between the transmitter- and receiver-side nodes can be clearly maintained. The weather was cloudy during the experiment. Note that mmWaves have been used as an alternative for backhaul, short-range and high-capacity indoor communications, and radar. Compared with the radio-frequency bands currently widely used, additional attenuation in the mmWave link budget, such as rain, oxygen, and hydrophilic materials (e.g., trees, leaves, and humans) must be considered. Note that radio waves in the 60-GHz band are particularly affected by the rain and oxygen. Nevertheless, the weather did not significantly affect network performance, and

TABLE I. MCS SETTINGS IN SINGLE CARRIER PHYSICAL MODE

Index	*Modulation method*	*Code rate*	*Repetition*	*Data rate* (Mbit/s)
1	BPSK	1/2	2	385
2	BPSK	1/2	1	770
3	BPSK	5/8	1	963
4	BPSK	3/4	1	1,155
5	BPSK	13/16	1	1,251
6	QPSK	1/2	1	1,540
7	QPSK	5/8	1	1,925
8	QPSK	3/4	1	2,310
9	QPSK	13/16	1	2,503
10	16-QAM	1/2	1	3,080
11	16-QAM	5/8	1	3,850
12	16-QAM	3/4	1	4,620

TABLE II. PHYSICAL-LAYER INFORMATION IN EXPERIMENT

Terms	*Antennas are matched*	*Antennas are mis-matched*
Radio channel	Ch 2 (60.48 GHz with 2.16 GHz)	
RSSI	-64 dBm	-62–63 dBm
MCS settings	8–9	6–9
Beam index	30 / 30	30 / 5

the beam direction was severely affected, as indicated by the experimental results [8]. Namely, the experiment was conducted in two scenarios: one in which both elevation and azimuth angles were appropriately adjusted (the antennas were matched), and the other in which they were slightly offset (the antennas were mismatched).

B. Experimental results: Network performance

Figure 11 shows the experimental results, which include both (a) and (b), (c) and (d), and (e) and (f) are TCP with the CUBIC algorithm, UDP, and ICN performance, respectively. In Figures 11(a) to (d), iPerf3 [36] was used to measure TCP/UDP performance at every 1 s interval for 90 s. Figures 11(e) and (f) show the results of retrieving the different data using Cefore. The status information of the physical layer for these scenarios is summarized in Table II. Note that, in the CNLR device, the antenna's front space is divided into a grid pattern of elevation- and azimuth- angles, and each sub-region is assigned a beamforming index. The most central beam direction on the antenna surface is when the beamforming index is 30.

As shown in Figure 11(a), the average TCP throughput was 941 and 94.4 Mbit/s when the antennas were matched and mismatched, respectively. The TG antenna is a parabolic dish; thus, even a few degrees of angular misalignment can cause significant degradation in TCP throughput. For TCP congestion control, as shown in Figure 11(b), the average congestion-window sizes were 1.26 and 0.967 Mbytes; hence, there was a 39.3% difference. In the curve, when the antennas were matched, several attempts were made to increase the congestion-window size.

As shown in Figure 11(c), the average UDP throughput was 902 and 93.3 Mbit/s for the two scenarios, respectively. In the curve, when the antennas were matched, there were

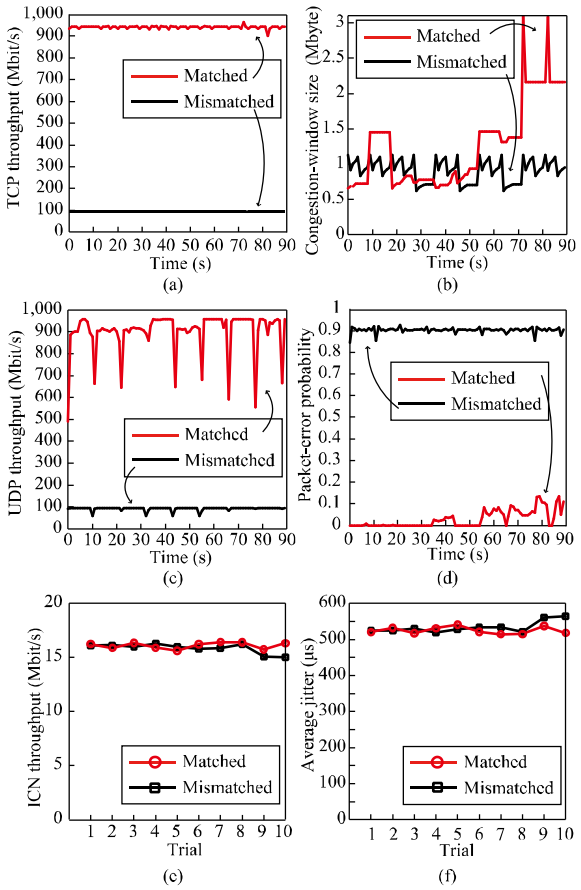

Figure 11. Experimental results in actual city

regions where UDP throughput temporarily decreased. The reason for this decrease is that automatic retransmission requests and forwarding-error-control mechanisms are omitted, resulting in these dramatic degradations. The results in Figure 11(a) indicate no degradation, as the TCP congestion control mechanism is available and effective. Figure 11(d) shows the packet-error probability for UDP transfer; the averages were 0.0294 and 0.903 for the matched and mismatched scenarios, respectively. When the antennas were mismatched, many packet losses occurred, affecting not only UDP throughput but also TCP throughput, as shown in Figures 11(a) and (c).

As shown in Figure 11(e), the average ICN throughput was 16.1 and 15.8 Mbit/s for the two scenarios, respectively. The ICN throughput was significantly smaller than that of TCP or UDP because Cefore has a bottleneck. In mmICWSN, the ICN layer was stacked on the TCP/UDP layers. Thus, due to the middleware implementation in Cefore, if the maximum data-transmission bandwidth is set to its maximum value, the failure probability of data registration, storage, and transfer worsens. As shown in Figure 11(f), the average jitter was 525 and 534 μs for the two scenarios, respectively. ICN throughput and jitter did not significantly differ between the two scenarios. In line with these results, we found that

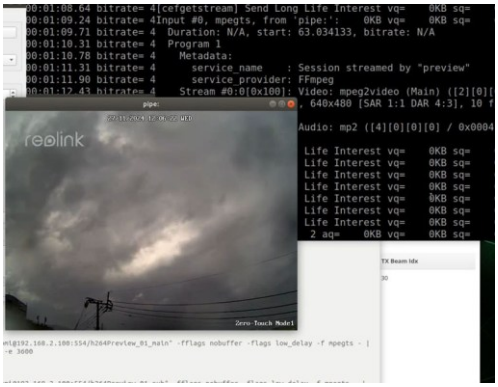

Figure 12. Experimental results regarding video-streaming demonstration in the long-distance environment

TCP/UDP/IP protocol stacks were not affected by the ICN-layer protocol. We also experimentally verified that we could obtain sufficient network performance for mmICWSN in an actual city.

C. *Experimental results: Video-streaming demonstration*

Similar to Section IV.C, the video-streaming experiment was conducted. As shown in Figure 9, the camera was located on the device at the community center, and the device received the video stream at the school. Figure 12 shows the experimental result in which the cefgetstream and sefputstream commands in Cefore were used to transmit and receive real-time video streams. Under matched and mismatched conditions, the video stream was delivered and received smoothly. Although there were differences in UDP network performance between the two conditions, the ICN performance did not differ. Therefore, we can conclude that the degradation in network performance did not affect the ICN layer for video-streaming applications.

VI. COMPUTER SIMULATION

In this section, the computer simulations regarding the frame-error-probability performance of mmWaves were performed. As a simulation environment, Mathworks Matlab (2025b) on a PC (Panasonic Let's Note FV1 (Core i7 1185 G7 (4-core, 3 GHz), 32-GB RAM, and Windows 11 Pro OS) was used. The parameter settings of the transceiver and receiver were determined based on the previous experiments. Namely, for the simulation scenario between ARNs, the height between the transmitter and receiver was set as 4.2 m, and their distance was set as 10, 20, and 30 m, respectively. In addition, as in the case of ARN and SN, the heights of the transmitter and receiver were set to 4.2 m and 1.2 m, respectively, and the distance between them was set to 20 m. The antenna has a 16 (= 4×4) element-based array layout, and the two antenna surfaces are placed face-to-face between the transmitters and receivers. In addition, we assume that the beamforming mechanism ideally works. In the radio-propagation environment, the transmission-side device is regarded as an access point (hotspot), located in an open space, and the receiver-side device is connected to it. For the wireless channel model, there was no terminal movement, including

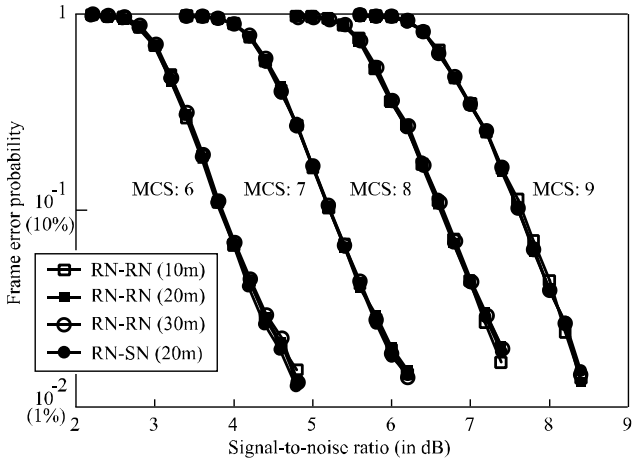

Figure 13. Computer-simulation result: frame-error probability versus signal-to-noise ratio in decibel

transmitter and receiver; thus, we assume it as an Additive White Gaussian Noise (AWGN) channel. In adaptive rate control, the MCS index was evaluated based on the actual observed values in Section IV B, specifically for the range of 6–9.

The computer simulation was based on exhaustive Monte Carlo simulations, with the number of iterations set to either 1,000 frame error detections or 10,000 frame transmissions. In addition, the frame length was set as 4,096 bytes (= 32,768 bits). Figure 13 shows the results of the frame-error probability versus the Signal-to-Noise Ratio (SNR) in decibels. As shown in Figure 13, the curves for the four cases were overlapped (similar); therefore, there is no difference between the node distances in these cases. The desired SNR at a frame error rate of 10% and 5% were 3.8, 5.2, 6.6, and 7.7 dB, and 4.2, 5.5, 7.0, and 8.0 dB for the case where the index of MCS was 6, 7, 8, and 9, respectively.

VII. Conclusion and Future Work

This paper evaluated and presented the feasibility of the network performance in the TCP, UDP, and ICN protocols with mmICWSN framework. The experimental results indicated that it was necessary to improve the ICN throughput by modifying the Cefore settings, and the antenna placement for mmWaves was sensitive to a few degrees of angle. Through the demonstration of the mmWaves experiment, the developed system could be applicable to multi-hop aerial nodes and long-distance wireless transmission in an actual city. For future work, we plan to deploy mmICWSN for practical smart-city applications, such as smart agriculture. In detail, we will develop a new ecosystem that supports an on-demand and real-time video and image forwarding platform for common demand in smart agriculture applications.

Acknowledgments

This work was partly supported by JSPS KAKENHI Grant Number JP25K15104 and NICT Japan, Grant Number JPJ012368C05601. We are grateful to Dr. Kenji Kanai and Dr. Taku Yamazaki for their helpful discussions, and to Nogata City and Advantech Japan for their help with the experiments.

References

[1] S. Mori, “Network-performance evaluation for millimeter-wave information-centric wireless-sensor-network ecosystem in actual city,” *Proc. IARIA ICN 2025*, pp. 7–11, Nice, France, May 2025.

[2] P. Mishra and G. Singh, “6G-IoT framework for sustainable smart city: Vision and challenges,” *IEEE Consumer Electronics Mag.*, pp. 1–8, Sept. 2023.

[3] B. Ahlgren, C. Dannewitz, C. Imbrenda, D. Kutscher, and B. Ohlman, “A survey of information-centric networking,” *IEEE Communications Mag.*, vol. 50, no. 7, pp. 26–36, July 2012.

[4] L. C. M. Hurali and A. P. Patil, “Application areas of information-centric networking: State-of-the-art and challenges,” *IEEE Access*, vol. 10, pp. 122431–122446, Nov. 2022.

[5] K. Aldubaikhy, W. Wu, N. Zhang, N. Cheng, and X. Shen, “MmWave IEEE 802.11ay for 5G fixed wireless access,” *IEEE Wireless Communications*, vol. 27, no. 2, pp. 88–95, Apr. 2020.

[6] S. Mori, “Test-field development for ICWSNs and preliminary evaluation for mmWave-band wireless communications,” *Proc. IEEE CCNC 2024*, Las Vegas, USA, Jan. 2024, pp. 1–2, doi: 10.1109/CCNC51664.2024.10454799.

[7] S. Mori, “Air-to-ground-integrated wireless information-centric networks with mmWave communications: Long-term operational testing and aerial node evaluation,” *Proc. IEEE APWCS 2024*, Singapore, Aug. 2024, pp. 1–5, doi: 10.1109/APWCS61586.2024.10679312.

[8] S. Mori, “Development of UAV-aided information-centric wireless sensor network platform in mmWaves for smart-city deployment,” *International J. Advances in Networks and Services*, vol. 17, no. 3&4, pp. 105–115, Dec. 2024.

[9] O. J. Adeleke, K. D. Jovanovich, S. Ogunbunmi, O. Samuel, and T. O. Kehinde, “Comprehensive exploration of smart cities: A systematic review of benefits, challenges, and future directions in telecommunications and urban development,” *IEEE Sensors Reviews*, vol. 2, pp. 228–245, May 2025.

[10] F. Tariq et al., “A speculative study on 6G,” I*EEE Wireless Communications*, vol. 27, no. 4, pp. 118–125, Aug. 2020.

[11] M. Alsabah et al., “6G wireless communications networks: A comprehensive survey,” *IEEE Access*, vol. 9, pp. 148191–148243, Nov. 2021.

[12] M. Vaezi et al., “Cellular, wide-Area, and non-terrestrial IoT: A survey on 5G advances and the road toward 6G,” *IEEE Communications Surveys & Tutorials*, vol. 24, no. 2, pp. 1117–1174, Feb. 2022.

[13] T. Ferreira et al., “Millimeter-wave feasibility in 5G backhaul: A cross-layer analysis of blockage impact,” *IEEE Access*, vol. 11, pp. 5178–5192, Jan. 2023.

[14] M. G. Doone et al., “Signal propagation characteristics at 6 GHz and 60 GHz for Wi-Fi 8 UHR in future factories,” *Proc. AP-S/INC-USNC-URSI 2024*, Firenze, Italy, July 2024, pp. 2189–2190, doi: 10.1109/AP-S/INC-USNC-URSI52054.2024.10687229.

[15] M. Zhang et al., “Will TCP work in mmWave 5G cellular networks?,” *IEEE Communications Mag.*, vol. 57, no. 1, pp. 65–71, Jan. 2019.

[16] E. Khorov, A. Krasilov, M. Susloparov, and L. Kong, “Boosting TCP & QUIC performance in mmWave, Terahertz, and Lightwave wireless networks: A survey,” *IEEE Communications Surveys & Tutorials*, vol. 25, no. 4, pp. 2862–2891, Aug. 2023.

[17] R. Kumar et al., “TCP BBR for ultra-low latency networking: Challenges, analysis, and solutions,” *Proc. IFIP Networking 2019*, Warsaw, Poland, May 2019, pp. 1–9, doi: 10.23919/IFIPNetworking.2019.8816856.

[18] R. Poorzare and A. C. Augé, “How sufficient is TCP when deployed in 5G mmWave networks over the urban deployment?,” *IEEE Access*, vol. 9, pp. 36342–36355, Mar. 2021.

[19] Z. Zhang et al., "In-network caching for ICN-based IoT (ICN-IoT): A comprehensive survey," *IEEE Internet of Things Journal*, vol. 10, no. 16, pp. 14595–14620, Aug 2023.

[20] C. Safitri, Q. N. Nguyen, M. Anugerah Ayu, and T. Mantoro, "Robust implementation of ICN-based mobile IoT for next-generation network," *Proc. IEEE ICCED 2022*, Sukabumi, Indonesia, July 2022, pp. 1–5, doi: 10.1109/ICCED56140.2022.10010561.

[21] G. Gür et al., "Integration of ICN and MEC in 5G and beyond networks: Mutual benefits, use cases, challenges, standardization, and future research," *IEEE Open Journal of the Communications Society*, vol. 3, pp. 1382–1412, Aug. 2022, doi: 10.1109/OJCOMS.2022.3195125.

[22] A. Pagano, D. Croce, I. Tinnirello, and G. Vitale, "A survey on LoRa for smart agriculture: Current trends and future perspectives," *IEEE Internet of Things Journal*, vol. 10, no. 4, pp. 3664–3679, Feb. 2023.

[23] M. N. Mowla, N. Mowla, A. F. M. S. Shah, K. M. Rabie, and T. Shongwe, "Internet of Things and wireless sensor networks for smart agriculture applications: A survey," *IEEE Access*, vol. 11, pp. 145813–145852, Dec. 2023.

[24] A. U. H. Hashmi et al., "Effects of IoT communication protocols for precision agriculture in outdoor environments," *IEEE Access*, vol. 12, pp. 46410–46421, Mar. 2024.

[25] Terragrah, https://terragraph.com/ (retrieved: Nov. 2025).

[26] BeMap, https://www.bemap.co.jp/ (retrieved: Nov. 2025).

[27] Cefore, https://cefore.net/ (retrieved: Nov. 2025).

[28] T. Yamazaki, S. Miyata, and T. Miyoshi, "A city airspace testbed for drone networks in future smart cities," *Advances in Engineering and Information Science Toward Smart City and Beyond*, pp. 141–162, May 2023.

[29] iPerf3, https://iperf.fr/ (retrieved: Nov. 2025).

[30] NGI, https://www.gsi.go.jp/ENGLISH/ (retrieved: Nov. 2025).